Available online at www.sciencedirect.com

SciVerse ScienceDirect

Procedia Engineering 58 (2013) 461 – 470

Procedia Engineering

www.elsevier.com/locate/procedia

The 12th Hypervelocity Impact Symposium

Implementation of Tillotson Equation of State for Hypervelocity Impact of Metals, Geologic Materials, and Liquids

Aaron L. Brundage*

Sandia National Laboratories, Integrated Military Systems Development Center, Albuquerque, NM 87185, USA

Abstract

The Tillotson equation of state (EOS), which was originally developed for the hypervelocity impact of metals, was augmented with an additional region in expansion to provide full coverage of the density-energy space and a new cavitation model for liquids. This EOS was implemented into CTH, Sandia National Laboratories Eulerian, finite-volume, shock physics code, for the general purpose of simulating hypervelocity impacts of metals, geologic materials, and liquids; however, the salient features of this EOS in both compression and expansion are evaluated for water given the ubiquity of available data. Addition of a cavitation model allows for treatment of liquid spall when the local pressure drops below the vapor pressure in events such as underwater blasts and high speed projectiles or fragments in liquids. The EOS is evaluated by comparing the response to previously published dynamic compression experiments. Additionally, the model results are compared against the Mie-Gruneisen and SESAME equations of state already in the CTH database.

Selection and peer-review under responsibility of the Hypervelocity Impact Society

Keywords: shock physics; cavitation; vapor dome; CTH; Tillotson EOS

Nomenclature

a	Tillotson parameter
A	Bulk modulus (kbar)
b	Tillotson parameter
B	Tillotson parameter (kbar)
c	Sound speed (cm/s)
C	Specific heat (erg/gK)
E	Internal energy (erg/g)
H	Enthalpy (erg/g)
IC	Initial condition
k	Specific heat ratio
L	Length (cm)
P	Pressure (kbar)
R	Ideal gas constant (erg/gK)
u	Flyer velocity (cm/s)
T	Temperature (K)
x	Quality

* Corresponding author. Tel.: +1-505-284-2958; fax: +1-505-284-1373.
E-mail address: albrund@sandia.gov. Sandia National Laboratories is a multi-program laboratory managed and operated by Sandia Corporation, a wholly owned subsidiary of Lockheed Martin Corporation, for the U.S. Department of Energy's National Nuclear Security Administration under contract DE-AC04-94AL85000.

Selection and peer-review under responsibility of the Hypervelocity Impact Society
doi:10.1016/j.proeng.2013.05.053

X	Dimension (cm)
Y	Dimension (cm)
Greek symbols	
α	Tillotson parameter
β	Tillotson parameter
Γ	STP Gruneisen parameter
η	Compression, ρ/ρ_0
μ	Strain, η-1
ρ	density (g/cm^3)
Subscripts	
0	Initial condition
1	Eqn. (1)
2	Eqn. (2)
3	Eqn. (3)
C	Cold state
cav	cavitation
CV	Complete vaporization
e	Electronic term
f	liquid state
g	gaseous state
H	Hugoniot
IV	Incipient vaporization
l	liquid
T	Thermal state
V	Volume

1. Introduction

The Tillotson Equation of State (EOS) was formulated originally for hypervelocity impact, recognizing that melting or vaporization can occur in the target or the flyer [1]. Under these extreme impact conditions, material response can span from low pressures, where strength effects dominate to very high pressures, where changes in chemical or electronic structure can occur. High states of expansion following shock compression can also be produced as relief waves arrive from free surfaces. Hence, the intent of the original Tillotson EOS was to present a simple model that included phase change processes by incorporating both low-pressure and high-pressure regions as part of the thermodynamic description. McQueen and Walsh [2] demonstrated that for metals shocked up to 2 Mb, mixed phases such as solid-solid phase transitions in Fe, Bi, and Sn, can occur upon shocking, and melting or incipient vaporization can occur upon release, especially for softer metals such as Cd, Pb, and Zn. A number of the metals described by this McQueen and Walsh [2] reference were characterized for hypervelocity impact by Tillotson [1]; however, at the higher impact velocities, the standard Mie-Gruneisen EOS was generalized to include high temperature effects, where the Gruneisen coefficient was assumed to be dependent upon two thermodynamic state variables—specific volume (or density) and internal energy. Although the solid-solid phase transformations can be included upon shock, as demonstrated by Ahrens [3] by augmenting the internal energy, no phase transformations are included upon compression in the original model; the material remains in the original solid phase and does not cross additional phase boundaries.

There are a number of limitations with the Mie-Gruneisen EOS [4]. Although widely used for many shock compression analyses of simple compressible substances, when the Hugoniot is used as the reference state, it is not valid for highly compressed states, nor is it applicable for expanded liquid or vapor states. When dissociation or thermal electronic excitation processes occur, the Gruneisen coefficient is no longer a single function of density, but must also include internal energy. Generally, this coefficient is a weak function of density with the exception of changes in electronic configuration or phase changes.

The Tillotson EOS surface has separate regions for compression and expansion. The compression region has validity to high pressures, where thermal electronic processes are permitted through a generalization of the Mie-Gruneisen EOS to fit Thomas-Fermi theoretical results [5]. In expansion, the EOS surface approaches ideal gas behavior at low densities. At energies below the sublimation energy, the gas-solid mixing region is approximated; however, liquid-gas, solid-liquid, and polymorphic solid-solid coexistence regions are not included.

The Thomas-Fermi statistical model, used to capture ionization effects, is valid in the high density asymptotic limit for metals. According to Asay and Kerley [6], this model has been used to compute the high pressure and temperature region of many existing tabular SESAME tables. At high densities, Fermi statistics are used to compute the energy of an average configuration of non-interacting atoms, versus calculations for isolated ones, since electron-electron interactions are nearly independent of configuration for metals.

Thomas-Fermi statistics only become important for temperatures far exceeding an electon volt and pressures well above a Megabar. Examples of situations where these extreme states can be reached include hypervelocity impacts of meteorites, space debris, or other flying objects onto planetary land mass or oceans, stars, or spacecraft. For example, thin layers designed to protect a spacecraft from hypervelocity meteor impact by designing the first target material to vaporize upon impact and have debris shielded from the spacecraft by a second target material represents a concept called a Whipple shield, named after the scientist who first designed it before the first US mission to space [7]. A debris cloud is formed from spall in both the target and projectile from intersecting rarefaction waves, as shown schematically by the impact of right circular cylinder into a thin plate [8]. A body of literature has been devoted entirely to debris cloud experiments and simulation [8-10].

The diameter and depth of impact craters on the earth, the ejecta near the crater, and other forensic information are often used in conjunction with a hydrocode to estimate impactor dimensions and flight conditions [10]. Depending upon these impact conditions, it could be determined that a considerable fraction of the energy was transferred to the atmosphere and some of the ejecta exceeded the escape velocity of the earth. For impacts into oceans, this could potentially cause tsunamis, endangering the lives of nearby island communities. At the impact plane, prompt vaporization of the liquid could occur, and at low pressure regions, such as those formed by colliding rarefaction waves, liquid spall or cavitation could also occur. (Cavitation is defined as the study of gaseous cavities that grow and collapse in a liquid [11]). In underwater explosions [12], vaporization or ionization occurs near the interface formed between the water and the explosive detonation products, and cavitation occurs locally as a result of release to pressures at or below the vapor pressure of water. Hence, it is valuable to have an equation of state with separate regions of compression and release. Since a vapor cannot support tension, a cavitation model is needed to capture the effects of liquid spall, where gaseous cavities are introduced as the fluid tears, and to prevent the development of unphysical negative pressures in this flow regime.

The remainder of this report contains a mathematical description of the original Tillotson EOS, with new improvements to the model that extends the ρ-E phase space and presents a solution strategy applicable to multidimensional hydrocode calculations. Furthermore, a new cavitation model, comparison of the model predictions to a subset of experimental data, a discussion of the results, and summarizing conclusions and recommendations for future research are also given.

2. Equation of State Modeling

2.1. Tillotson EOS

The Tillotson EOS represents an analytic thermodynamic P-ρ-E surface which is applicable to the prediction of the shock and release of materials undergoing hypervelocity impacts [1]. This EOS represents an improvement over the classical Mie-Gruneisen equation of state for compressed states by assuming a Gruneisen coefficient Γ as a function of both density and energy, whereas the classical description, derived from microstructural atomic lattice models [4], features Γ as a function of density. The linear shock velocity Hugoniot is recovered at low pressures (and energy) and the Thomas-Fermi atomistic model is asymptotically reached at high pressures (and energy) during shock compression. For compressed states this pressure is given by

$$P(\rho,E)=\left[a+\frac{b}{\left(E/\left(E_0\eta^2\right)+1\right)}\right]\rho E+A\mu+B\mu^2 \qquad \left(\rho\geq\rho_0, E\geq 0\right). \tag{1}$$

In expansion, the revised Tillotson EOS is represented by four separate regions, identified by the individual liquid (or solid) or gaseous phase and a mixed phase region. In the first expansive region, the material density is less than the reference/initial density, but greater than the density at incipient vaporization. Likewise, the energy is less than the internal energy at incipient vaporization, so it remains a liquid (solid). Hence, for cold expanded states, the EOS is given by

$$P(\rho,E)=\left[a+\frac{b}{\left(E/\left(E_0\eta^2\right)+1\right)}\right]\rho E+A\mu+B\mu^2 \quad \left(\rho_0>\rho\geq\rho_{IV},E\leq E_{IV}\right). \tag{2}$$

For hot expanded states where the material has completely vaporized, a separate expression for the pressure is given by

$$P(\rho,E)=a\rho E+\left\{\frac{b\rho E}{\left(E/\left(E_0\eta^2\right)+1\right)}+A\mu e^{-\beta[(\rho_0/\rho)-1]}\right\}e^{-\alpha[(\rho_0/\rho)-1]^2} \quad \left(\rho_0>\rho,E\geq E_{CV}\right). \tag{3}$$

As the density approaches zero, the second term in the above expression vanishes and the material approaches the classical Thomas-Fermi limit [5],

$$P_e=\rho\Gamma_e E_e \quad \left(\rho_0\gg\rho,E\gg E_{CV}\right), \tag{4}$$

where Γ_e equals 2/3 for a free electron gas and 0.5 for a real gas. The pressure P_3 given in Eqn. (3) is chosen to match the value P_2 in Eqn. (2) at the initial density; however, at slightly smaller densities, the pressures become discontinuous. Although Tillotson [1] cautions about the discontinuity, no expressions are given to rectify the discontinuity. In later citations [13, 14] for example, a mixing region between the gas and liquid (solid) was defined as

$$P(\rho,E)=\frac{(E-E_{IV})P_3+(E_{CV}-E)P_2}{E_{CV}-E_{IV}} \quad \left(\rho_0>\rho>\rho_{IV},E_{IV}<E<E_{CV}\right). \tag{5}$$

It should be noted that the mixing region does not represent a vapor dome for the case of liquid/vapor mixture. As demonstrated later, above the critical point, there is just a fluid, a critical fluid, which is liquid/vapor mixture. By no means does the model intend to match critical behavior; it should be treated as a mixture between two phases using a simple mixing rule. Specifically capturing the coexistence regions in the model would require implementing separate solid-liquid and liquid-vapor equations of state, as exemplified by Royce for the Gray EOS [15] for metals. Finally, for representing low energy expansion states in the Tillotson model, an additional term was added such that

$$P(\rho,E)=\left[a+\frac{b}{\left(E/\left(E_0\eta^2\right)+1\right)}\right]\rho E+A\mu \quad \left(\rho<\rho_{IV},E<E_{CV}\right). \tag{6}$$

Tillotson [1] uses this exact form to estimate the density at incipient vaporization; however, it is not identified as a separate region in the original paper. The internal energy E is comprised of contributions from the liquid (solid) at zero-Kelvin, and thermal and electronic contributions [5], as given below

$$E(\rho,T)=E_C(\rho)+E_T(\rho,T)+E_e(\rho,T), \tag{7}$$

where $E_T=C_V T$ and $E_e\approx 0$ (small relative to the other terms) for the range of temperatures and pressures in this paper. In compression, the cold curve is defined as

$$\frac{dE_C}{d\rho}=\frac{P_1(\rho,E_C)}{\rho^2} \quad \left(IC:\rho=\rho_0,E_C=0\right), \tag{8}$$

where this equation is solved numerically for the cold curve using a fourth-order Runge-Kutta scheme. The same methodology is used to solve the cold curve in expansion, with the exception that the right hand side of the equation is a piecewise function of Eqns. (2, 3, 5, 6). These equations are implemented in the Eulerian shock physics code CTH [16]. In the literature, it is not clear how energy is treated in the Tillotson EOS, or if the EOS was evaluated at states other than along the Hugoniot. In some references, only the compressed states given by Eqn. (1) or a linearized version of this relationship is implemented in the computational tool [12, 17].

For evaluating the Tillotson EOS in CTH, the results from a 1D impact simulation, giving Hugoniot end states, were compared against other models in CTH (Mie-Gruneisen and a tabular SESEME EOS) and published compression data for water. For brevity, the equations for Hugoniot pressure and energy are omitted from this paper; the reader is directed to Ahrens and O'Keefe [3] for those relationships. The Hugoniot temperature is calculated from the Hugoniot energy and cold curve, as given in the following equation

$$T_H(\rho) = T_0 + \frac{E_H(\rho) - E_C(\rho)}{C_V} \quad (\rho \geq \rho_0). \tag{9}$$

To evaluate the shock states in CTH along the Hugoniot, a simple set of one-dimensional (1D) simulations in which a flyer (water) of thickness L = 3 cm impacted a target of thickness 2L for flyer velocities u up to 9×10^5 cm/s, as shown in Fig. 1. The shock states were evaluated at the impact surface. This setup has the dual purpose of evaluating spall leading to cavitation at the spall plane located the mid-plane within the target.

Comparison of the analytical Hugoniot pressure, CTH shock states predicted with the Tillotson, Mie-Gruneisen and SESAME equations of state, and measurements of the Hugoniot pressure up to 400 kbar are plotted in Fig. 2.

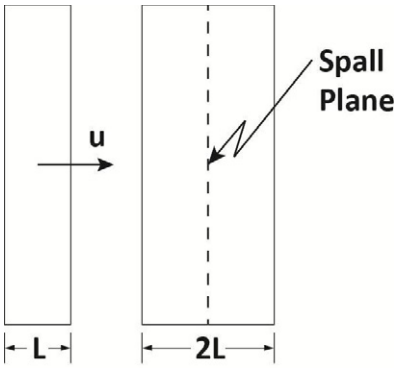

Fig. 1. Schematic of impact configuration in CTH for evaluating shock Hugoniot end states and release using Tillotson equation of state.

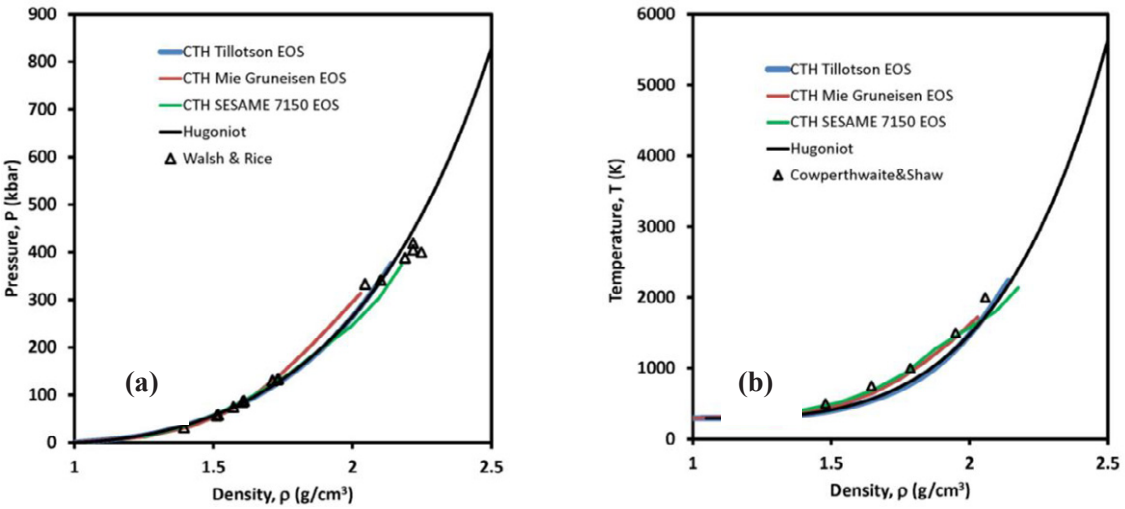

Fig. 2. Comparison of analytical, CTH output for two common models, and measurements of the (a) pressure and (b) temperature along the shock Hugoniot for water.

The analytical Hugoniot curve and the Tillotson EOS pass through the data, giving a similar fit to that of Walsh and Rice [18], as shown in Fig. 2(a). The tabular EOS for water [19] follows the Hugoniot curve, then changes slope, which is indicative of predicted phase change. Unfortunately, the SESAME EOS for water has a number of deficiencies, mainly being sparsely populated and providing a poor representation of the two-phase saturated region. It is also inadequate for modeling cavitation, where the flow could expand to extremely low pressures (e.g. 0.006 bar). Both the Mie-Gruneisen and Tillotson equations of state assume a constant specific heat; the primary difference between these equations of state are the representation of the Gruneisens' coefficient, where the Tillotson EOS assumes a more general form having a dependence on both energy and density. Beyond 100 kbar, the slope of the Mie-Gruneisen Hugoniot pressure increases, and this EOS predicts higher pressures for the same compression. All of the equations of state provide a good match with the pressure data, given the scatter in the points. In comparing the temperatures in Fig. 2(b), it is clear that the tabular equation of state, which has variable specific heat, provides the best fit to the temperature measurements [20]. According to Cowperthwaite and Shaw [20], specifying specific heat as a function of temperature is adequate for predicting the correct thermal response. The Mie-Gruneisen also predicts the measured temperature response up to 1500 K; however, the excellent match to the data is a consequence of slightly overpredicting the hydrodynamic response and not representative of improved physics, as in the SESAME EOS. Beyond a compression of ratio of two, both the Mie-Gruneisen and SESAME EOS intersect and overshoot the temperature Hugoniot; yet, the Tillotson EOS continues to track the Hugoniot curve computed according to Eqn. (9). Hence, one area of improvement for both the Mie-Gruneisen and Tillotson equations of state to provide the best match to the data is to reformulate with a variable specific heat. This is very important for liquids, where shock temperatures are sensitive to specific heat and specific heat increases with pressure, as explained by Cowperthwaite and Shaw [20]. The Mie-Gruneisen EOS in terms of specific heat as a function of temperature was presented by Baer *et al*. [21].

2.2. Cavitation Modeling

An engineering approach to modeling cavitation is to consider a simple model where water is assumed to cavitate if the pressure falls below a certain cutoff value, equal to the vapor pressure [22]. This type of approach introduces a discontinuity across the vapor bubble. More sophisticated approaches are available, such as assuming a baratropic flow where the density across the bubble is assumed to be a function of pressure only to a multiphase approach, where separate equations are solved for liquid and vapor regions. A detailed overview of the variety of available methods for modeling cavitation is summarized by Saurel and Petipas [23].

In the model presented herein, cavitation is assumed to occur only upon release for densities less than ρ_0 and positive pressures. The model reproduces states along the isotherm ($T = T_{cav}$) within the vapor dome [24] between the endpoint on the saturated liquid line (ρ_{cav}, P_{cav}) and the corresponding endpoint on the saturated vapor line, as shown in Fig. 3.

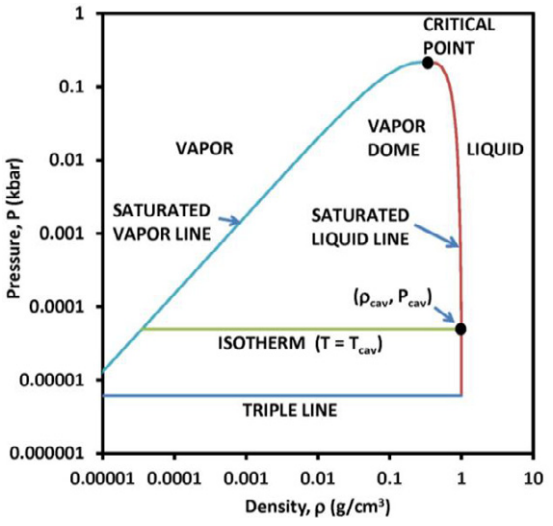

Fig. 3. Pressure-density diagram for water showing liquid and vapor phases, and saturated states for cavitation model. Vapor dome data from Van Wylen and Sonntag [24].

The Tillotson EOS uses a separate EOS for release instead of simply reflecting about the shock Hugoniot and releasing to ρ_0. Hence, the cutoff values for pressure and the energy, which will be a function of density and cavitation temperature, are given by

$$P(\rho,E) = P_{cav} \quad (\rho < \rho_0), \tag{10}$$

$$E(\rho,T) = E_C(\rho) + C_V T \quad (\rho < \rho_0, T = T_{cav}). \tag{11}$$

The sound speed in the cavitated region is defined by mixing the sound speed in the liquid and gas per Schmidt's rule [25], such that

$$x = \frac{\rho - \rho_0}{\rho_g - \rho_0} \quad (\rho < \rho_0, T = T_{cav}) \tag{12a}$$

$$c_g = \sqrt{\frac{k * P_{cav}}{\rho_g}} \tag{12b}$$

$$\frac{1}{\rho c^2} = \frac{x}{\rho_g c_g^2} + \frac{1-x}{\rho_0 c_l^2} \tag{12c}$$

Additional tests of the model with 1D spall simulations of water (see Fig. 1) were conducted at impact speeds of 2×10^5 cm/s, 3×10^5 cm/s, and 8×10^5 cm/s. From these simulations, the various release paths followed by the water at the target's mid-plane were plotted to assess whether spall leading to cavitation had been predicted by the Tillotson EOS model. These results are provided in Fig. 4.

According to the figure above, cavitation occurs at the spall plane from initial flyer impacts at 2×10^5 cm/s and 3×10^5 cm/s. For these release states, only a minute mass fraction of vapor is formed, which is consistent with the formation of initially small bubbles. At the higher impact velocity of 8×10^5 cm/s, the internal energy is greater than the energy required for complete vaporization and the fluid releases into a superheated region.

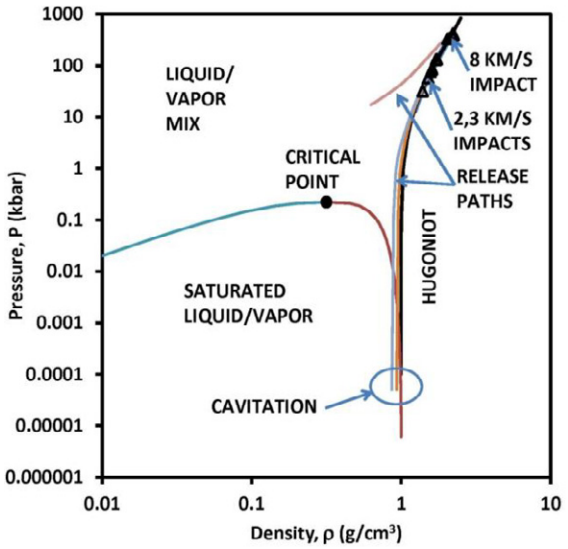

Fig. 4. Release paths from shock Hugoniot end states due to water-water impacts at 2×10^5 cm/s, 3×10^5 cm/s, and 8×10^5 cm/s.

Table 1. Tillotson Equation of State Parameters for Water

ρ	ρ_{IV}	a	b	A	B	E_0	α	β	E_{IV}	E_{CV}
(g/cm^3)	(g/cm^3)	(--)	(--)	kbar	kbar	10^{12}erg/g	(--)	(--)	10^{12}erg/g	10^{12}erg/g
0.998	0.958	0.7	0.15	21.8	132.5	0.07	10	5	0.00419	0.025

Table 2. Cavitation Parameters for Water

ρ	ρcav	P_{cav}	T_{cav}	k	R	C_V	H_{fg}
(g/cm^3)	(g/cm^3)	kbar	(K)	(--)	erg/g-K	erg/g-K	10^{12}erg/g
0.998	0.995	5.00E-05	305.9	1.33	4.62E+06	3.69E+07	2.42E-02

2.3. Underwater Explosion Modeling and Results

Understanding the fluid-structure interaction on underwater or free surface structures due to underwater explosions is generally complicated by resolving the wide range of length and time scales from the formation and collapse of small bubbles to the dynamic behavior of ships, submarines, and other submerged structures of interest in the far-field [26]. Small scale experiments and complementary modeling provide a cost-effective solution to developing a predictive capability towards gaining confidence in estimating the damage of underwater structures from complex shock and bubble interactions. A simple experiment where an explosive charge is placed in a well instrumented water-filled can has been used over the years for model validation experiments, as described by Wardlaw *et. al* [12, 27]. These experiments are used to evaluate the Tillotson EOS and cavitation model implemented in CTH; however, a complete model validation is not presented herein, just a description of how the new model improves the prediction of cavitation and bubble dynamics. Apart from understanding underwater fluid-structure interactions from underwater explosions, having a model that is applicable to hypervelocity impacts and high-speed projectiles, as well as biological applications such as the low-speed impacts on the human head leading to Traumatic Brain Injury (TBI), where bubble collapse in the head might be a contributor to irreversible damage and bruising, is an emerging field study that can benefit from implementation of a cavitation model in a shock physics code [28, 29].

Results from the CTH simulations of the hydrobulge test case is shown in the panel plot of Fig. 5, where the dynamics of the initial bubble formation is captured. Vapor bubble growth begins at the water/wall interface, as the shock wave releases from the surface, causing initial deformation from blast loading.

In Fig. 6, release paths are shown from two tracers (X, Y) = (0.88, 0) cm and (2.64, 0) cm located at the midplane between the explosive and the wall (X, Y coordinates are shown in Fig. 5). The one at (2.64, 0) cm cycles between release to the cavitation vapor pressure (P_{cav}) and compression to a state near or on the Hugoniot, as vapor bubbles are formed and collapsed. At the other location which is nearest to the explosive, a vapor bubble is repeatedly compressed, where the pressure oscillates around the critical point for water, and release states are computed on both sides of the saturated liquid line of the vapor dome. Given that the densities are less than that for the cavitated release states, the vapor volume is greater.

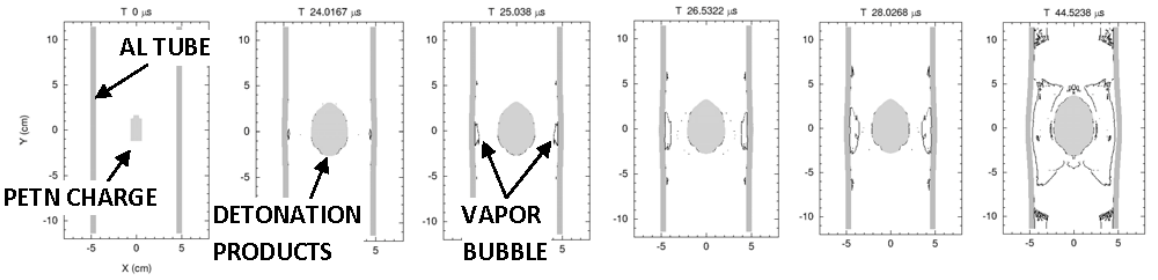

Fig. 5. Panel plot demonstrating the underwater detonation of a 2.8 g PETN charge initiated on top and the subsequent bulging and vapor bubble development on the interior surface an Aluminum tube over 44.5 μs.

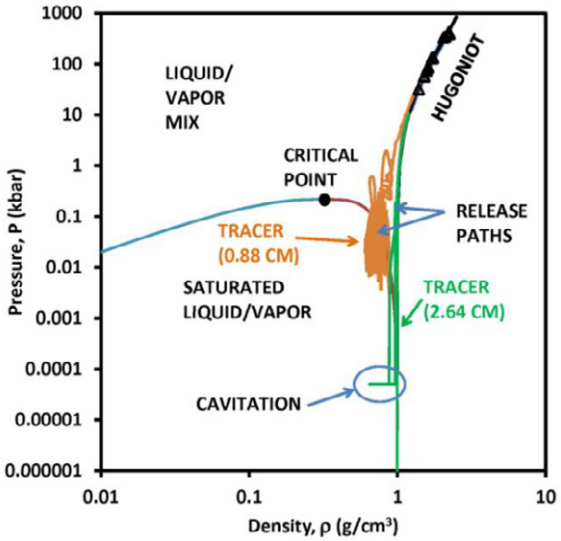

Fig. 6. Release paths from shock Hugoniot end states into water for hydrobulge simulation. Some of the release states cross the vapor dome to below 10^{-4} kbar simulating cavitation. Other release state into superheated liquid/vapor mixture region.

Although a cavitation model is needed to capture vapor formation at pressures at or below the vapor pressure of water, additional expanded states are captured by this modified Tillotson equation of state. Hence, models that use the same EOS for shock and release, where cavitation is assumed to occur for slightly compressed states at the vapor pressure of water, underpredict the vapor volume [12, 27]. It is the rapid collapse of these vapor bubbles which create intense pressure pulses that could potentially lead to structural damage of nearby underwater structures.

3. Conclusions and Recommendations

The Tillotson EOS and a cavitation model for water were implemented into CTH. This work represents an extension beyond the originally published phase space by incorporation of four separate expansion regions as well as the originally published compressive region. Shock Hugoniot pressure and temperature measurements are compared to the computations, and the model is generally within good agreement over the measurement range. The temperatures are underpredicted due to the assumption of constant specific heat; however, one area of future work would be to extend the model for variable specific heat. The Tillotson equation of state includes liquid (solid) regions, a vapor region, and a mixed region that is obtained by applying a simple mixture rule.

Cavitation behavior was modeled via a pressure cutoff model, where the flow is assumed to be cavitated if the pressure falls below the vapor pressure of water at the vapor temperature. In a numerical spall experiment, the model was shown to cavitate as expected, as illustrated by release paths from the Hugoniot. This same technique was also used to evaluate more complex bubble dynamics and fluid-structure interactions in an explosively-driven, water-filled can. Here, not all of the vapor that formed was assumed to have come from cavitation, but from release to a superheated liquid/vapor mixture. Models that only have the compressive region of the Tillotson EOS will predict release along a reflected Hugoniot to the reference state (assuming a single shock and release). Athough the water vapor dome was shown for convenience, the Tillotson EOS does not explicitly model gas-liquid and liquid-solid coexistence regions. The Tillotson EOS is also used for hypervelocity impacts into metals and geologic materials. Model fits for some of these materials are included in CTH, and for brevity, a demonstration of their fit to available shock Hugoniot and release adiabat data are not given herein. It should be noted that many geologic materials are porous and can undergo polymorphic phase transformations in both compression and expansion from hypervelocity impact. Approaches that account for phase change in hydrocode modeling of compression and release in metals and geologic materials is described in a number of references cited herein [3, 4, 13, 30]. This modified Tillotson EOS model assumes single phase behavior upon compression.

Acknowledgements

The author gratefully thanks the reviewers of this document for their insightful comments and suggestions.

References

[1] Tillotson, J.H., 1962. Metallic equations of state for hypervelocity impact. General Atomic Report GA-3216, General Atomic, San Diego, CA.
[2] McQueen, R. G., Marsh, S.P., 1960. Equation of State for Nineteen Metallic Elements from Shock-Wave Measurements to Two Megabars. Journal of Applied Physics 31, p. 1253.
[3] Ahrens, T.J., O'Keefe, J.D., 1977. Equations of State and Impact-Induced Shock-Wave Attenuation on the Moon. Impact and Explosion Cratering, D. J. Roddy, R.O. Pepin, and R.B. Merrill, Editors, Pergamon Press, New York, pp. 639-656.
[4] Rice, M.H., McQueen, R.G., Walsh, J. M., 1958. Compression of Solids by Strong Shock Waves. Solid State Physics, F. Seitz and D. Turnbull, Editors, Academic Press 6, pp. 1-63.
[5] Zel'dovich, Y.B., Raizer, Y.P., 1967. Physics of Shock Waves and High-Temperature Hydrodynamic Phenomena Volume II. W.D. Hayes and R.F. Probstein, Editors, Academic Press, New York, pp. 688-705.
[6] Asay, J.R., and Kerley, G.I., 1987, The Response of Materials to dynamic loading, International Journal of Impact Engineering 5, pp. 69-99.
[7] Buyuk, M., Kurtaran, H., Marzougui, D., Kan, C.D., 2008, Automated Design of Threats and Shields under Hypervelocity Impacts by using Successive Optimization Methodology, International Journal of Impact Engineering 35, pp. 1449-1458.
[8] Anderson, C.E. Jr., Trucano, T.G., Mullin, S.A., 1990. Debris Cloud Dynamics, International Journal of Impact Engineering 9, pp. 89-113.
[9] Trucano, T.G., Asay, J.R., 1987, Effects of Vaporization on Debris Cloud Dynamics, International Journal of Impact Engineering 5, pp. 645-653.
[10] Johnson, W.E., Anderson, C. E. Jr., 1987. History and Application of Hydrocodes in Hypervelocity Impact, International Journal of Impact Engineering 5, pp. 423-439.
[11] Arakeri, V.H., 1973, Viscous Effects in Inception and Development of Cavitation on Axi-Symmetric Bodies. Part I - Cavitation Inception. Part II - A Semi-Empirical Method to Predict Cavitation Separation on Smooth Bodies. Naval Ship Research and Development Center Report No. ENG 183-1 (AD-757 078), Bethesda, MD.
[12] Wardlaw, A., McKeown, R., Luton, J., 1999. Coupled Hydrocode Prediction of Underwater Explosion Damage, 48th Annual Bomb and Warheads Technical Symposium, Monterey, CA, May 11–14 (AD# A363434).
[13] Melosh, H. J., 1989. Impact Cratering. Oxford University Press, New York.
[14] Holian, K.S., Holian, B.L., 1989. Hydronamic Simulations of Hypervelocity Impacts, International Journal of Impact Engineering 8, pp. 115-132.
[15] Royce, E.B., 1971. Gray, A Three-Phase Equation of State for Metals. Lawrence Livermore Laboratory UCRL-51121, University of California, Livermore, CA.
[16] McGlaun, J. M., Thompson, S. L., and Elrick, M. G., 1990. CTH: A three-dimensional shock wave physics code, Int. J. Impact Engng. 10, pp. 351-360.
[17] Collins, G.S., Melosh, H. J.,Wunnemann, K., 2011. Improvements to the ε–α Porous Compaction Model for Simulating Impacts into High-Porosity Solar System Objects, International Journal of Impact Engineering 38, pp. 434-439.
[18] Walsh, J.M., Rice, M.H., 1957. Dynamic Compression of Liquids from Measurements on Strong Shock Waves. The Journal of Chemical Physics 26, pp. 815-823.
[19] Ree, F.H., 1976. Equation of State of Water. Lawrence Livermore Laboratory UCRL-52190, University of California, Livermore, CA.
[20] Cowperthwaite, M., Shaw, R., 1970. Cu(T) Equation of State for Liquids. Calculation of the Shock Temperature of Carbon Tetrachloride, Nitromethane, and Water in the 100kbar Region. The Journal of Chemical Physics 53, pp. 555-560.
[21] Baer, M.R., Gartling, D.K., DesJardin, P.E., 2011. Probabilistic Models for Reactive Behaviour in Heterogeneous Condensed Phase Media. Combustion Theory and Modeling 16:1, pp. 75-106.
[22] Jiang, J., Olson, M.D., 1996. Non-linear Transient Analysis of Submerged Circular Plates Subjected to Underwater Explosions. Computer Methods in Applied Mechanics and Engineering 134, pp. 163-179.
[23] Saurel, R., Petitpas, F., 2007. A Hyperbolic Non Equilibrium Model for Cavitating Flows. Fluid Dynamics of Cavitation and Cavitating Turbopumps, L. d'Agostino, M.V. Salvetti, Editors, CISM International Centre for Mechanical Sciences 496, Springer Vienna, pp. 279-316.
[24] Van Wylen, G.J., Sonntag, R.E, 1986. Fundamentals of Classical Thermodynamics, 3rd ed., John Wiley & Sons, New York.
[25] Ferrari, A., 2010. Modeling Approaches to Acoustic Cavitation in Transmission Pipelines, International Journal of Heat and Mass Transfer 53:19-20, pp. 4193-4203.
[26] Shin, Y.S., 2004. Ship Shock Modeling and Simulation for Far-Field Underwater Explosion. Computers and Structures 82, pp. 2211-2219.
[27] Wardlaw, A.B., Jr., Luton, J.A., 2000. Fluid-structure Interaction Mechanisms for Close-in Explosions. Shock and Vibration 7, pp. 265-275.
[28] Brennen, C.E., 2003, Cavitation in Biological and Bioengineering Contexts, 5th International Symposium on Cavitation, CAV2003, Osaka, Japan, pp. 1-9.
[29] Lubock, P., Goldsmith, W., 1980, Experimental Cavitation Studies in a Model Head-Neck System, Journal of Biomechanics 13, pp. 1041-1052.
[30] Shuster, S. H., Isenberg, J., 1972. Equations of State for Geologic Media. Defense Nuclear Agency Report No. DNA 2925Z, Defense Nuclear Agency, Washington, DC.